CrossMark

Na doping effects on the structural, conduction type and optical properties of sol–gel ZnO thin films

A. Chelouche[1] · T. Touam[2,5] · F. Boudjouan[1] · D. Djouadi[1] · R. Mahiou[3] ·
A. Bouloufa[4] · G. Chadeyron[3] · Z. Hadjoub[2]

Abstract In this work we report on the sol–gel deposition of Na doped ZnO thin films on quartz substrates. The effects of Na doping concentrations (0, 3, 6 and 9 at.%) on structural, morphological, electrical and optical properties of the synthesized films were systematically investigated by X-ray diffraction (XRD), Raman spectroscopy, atomic force microscopy (AFM), Hall-effect measurements, UV–Vis–NIR spectrophotometry and photoluminescence (PL) spectroscopy. XRD patterns showed that the prepared films were highly c-axis oriented exhibiting hexagonal wurtzite structure of ZnO. Raman spectra of All the ZnO films exhibited similar scattering peaks corresponding to the Raman active modes of ZnO wurtzite hexagonal structure. AFM images indicated that grain size and surface roughness of the films were affected by Na doping. From the Hall-effect measurements, it was found that carrier type is dependent on Na content. The UV–Vis–NIR spectroscopy analyses revealed that all the films were highly transparent in the visible region. Room temperature PL spectra demonstrated that UV emission of the Na-doped ZnO thin films depends on the Na concentration. In particular, the undoped sample shows the highest emission intensity, while the p-type Na doped ZnO film at 3 at.% exhibits the lowest one.

1 Introduction

ZnO has received considerable attention over the past years owing to its interesting properties such as a wide band gap (3.37 eV) and large exciton bending energy (60 meV) at room temperature. Thus, with such properties, ZnO would be a potential candidate for low-cost and highly efficient near-UV luminescent devices. In particular, ZnO nanostructures have been used for many technological application such as photovoltaic solar cell [1], light emitting diode [2] and photocatalytic activity [3].

However, growth of reproducible and stable p-type ZnO is essential to realize these applications. It was demonstrated that the achievement of p-type ZnO through impurity doping is rather difficult due mainly to the self-compensation effect from native defects [4]. Considerable efforts have been made to realize p-type ZnO using group I or group V elements as dopants. Theoretical investigations by Fan et al. [4] and Lee and Chang [5] have shown that group I elements as p-type dopants in ZnO are far better than group V elements. Among group I-elements, Na in Zn vacancy (Na_{Zn}) was theoretically predicted to occupy a shallow acceptor level [6]. Moreover, the bounding energy of Na–O (256 kJ/mol) is much greater than that of Zn–O (159 kJ/mol), which indicates a high stability of the Na_{Zn} acceptors [7]. Furthermore, Huang et al. [8] pointed out that it is possible to obtain stable p-type conductivity in Na-doped ZnO films because of the stable substitutional Na.

✉ A. Chelouche
azeddinechelouche@gmail.com

1 Laboratoire de Génie de l'Environnement, Faculté de Technologie, Université de Bejaia, 06000 Bejaïa, Algeria

2 Laboratoire des Semi-conducteurs, Université Badji Mokhtar, BP 12, 23000 Annaba, Algeria

3 Institut de Chimie de Clermont-Ferrand, UMR 6296 CNRS/UBP/Sigma Clermont, Université Clermont Auvergne, 63171 Aubière, France

4 Laboratoire d'électrochimie et Matériaux, Département d'électronique, Faculté de Technologie, Université Sétif-1, 19000 Sétif, Algeria

5 Unité de Recherche en Optique et Photonique, UROP – CDTA, Université Ferhat Abbas Sétif 1, 19000 Sétif, Algeria

Lee and Chang [5] found that the formation energy of substitutional Na (Na_{Zn}) is much lower than that of Na_i in O-rich condition. Park et al. [6] found that the position of defect energy levels of Na_{Zn} is 170 meV. Fan et al. [4] and Lin et al. [9] have reported that the presence of H and oxygen-rich conditions are necessary in order to achieve p-type doping in Na-doped ZnO.

P-type Na-doped ZnO nanostructures have been prepared using various methods such as pulsed laser deposition [10–14], magnetron sputtering [15, 16], plasma assisted molecular beam epitaxy [17], metalorganic chemical vapor deposition [18], continuous flow microreactor [19] and sol–gel process [20]. Among these techniques the sol–gel route offers a number of important advantages including lower equipment costs, lower processing temperatures, easy control of the composition at molecular level using different precursors as dopant sources and the possibility to use various substrates.

It should be noted that not only a few research works were reported on this subject but also no consensus has been reached; the published data are mostly controversial. For example, Lai et al. [20] have studied p-doping in ZnO: Na prepared by sol–gel process. They found that p-type is obtained at Na concentration of 15 and 20 at.%. Liu et al. [13] have reported that Na-doped p-type ZnO is obtained at Na concentration of 1 at.%. While Zheng et al. [11] have reported p-type ZnO at Na concentration of 2 and 5 at.%. Yang et al. [15] and Lin et al. [12] have prepared Na-doped ZnO thin film. They pointed out that p-type conduction is achieved at 1.0 and 0.5 at.% Na content.

In this context, the present investigation is intended to enrich our understanding of the effect of Na doping on the p-type conductivity since, to the best of our knowledge, only one work has been reported on p-type sol–gel Na-doped ZnO [20]. To do so, undoped and Na doped ZnO thin films were deposited onto quartz substrates using a sol–gel dip-coating process. A systematic study was carried out to reveal the effects of Na doping concentration on the structural, morphological, electrical and optical properties of the prepared films by using different characterization methods.

2 Experimental

2.1 Materials

Undoped and Na-doped ZnO thin films were prepared using the method reported in our previous works [21, 22]. Briefly, zinc acetate dehydrate ($Zn(CH_3COO)_2$, $2H_2O$) (sigma Aldrich) was first dissolved in 2-methoxyethanol. Monoethanolamine (MEA) (sigma Aldrich) was added to the solution in order to get MEA to Zn ratios of 1.0. The concentration of zinc acetate in the solution was kept at 0.4 M. For doped sols, anhydrous sodium acetate (sigma Aldrich) were added to the mixture to obtain sols with Na atomic concentrations fixed at 3, 6, and 9 at.%, respectively. All resultant ZnO sols were allowed to stand under continuous magnetic stirring at 50 °C for 1 h to get clear and homogeneous solutions. The obtained sols then aged at room temperature for 1 week. Prior to deposition, quartz substrates were washed with a liquid detergent, rinsed with distilled water, and then immersed in 4 M nitric acid for 24 h. They were then ultrasonically cleaned and rinsed in ethanol and distilled water during 15 min at 60 °C and, finally, were dried at 100 °C for 2 h. The deposition was carried out on quartz substrates using a KSV dip-coater with a withdrawal speed of 1.5 cm/min. After the dip coating, the samples were preheated at 400 °C for 10 min. This process of dip-coating and preheating was repeated eight times. The films were then heated up to 500 °C for 1 h in order to obtain crystallized ZnO.

2.2 Techniques

X-ray diffraction (XRD) analyses of the prepared films were performed on a PANalytical's MPD Pro X-ray diffractometer operating at 40 kV and 30 mA using the Cu Kα radiation (λ = 1.5406 Å). Raman study was carried out by using a T64000 Jobin Yvon confocal micro Raman spectrometer equipped with an Olympus microscope. The surface analyses were performed by a Bruker Innova Atomic Force Microscope. Hall-effect measurements were achieved at room temperature using an Ecopia HMS-5000 system in the Van der Pauw configuration. Optical transmittance spectra were obtained on a Shimadzu UV-2600 UV–Vis spectrophotometer. The photoluminescence properties were measured at room temperature using Xenon lamp operating at 350 nm. The incident beam was focused perpendicularly to the film surface and the fluorescence was collected in a guiding mode using a TRIAX 550 Horiba–JobinYvon monochromator equipped with a nitrogen cooled CCD camera.

3 Results and discussion

3.1 Structural and morphological properties

The structure of all prepared thin films was measured in the 2θ range 20°–60° at a resolution of 0.017° per step size. Figure 1 shows the XRD patterns of pure and Na-doped ZnO thin films at different Na doping level. It can be seen that all the films exhibit hexagonal wurtzite structures and the strong peak along [002] direction confirms that the ZnO is well crystallized and the crystallites are highly oriented
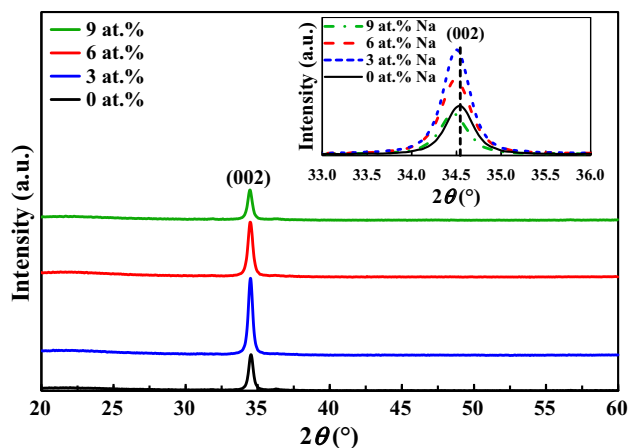
Fig. 1 XRD patterns of undoped and Na-doped ZnO thin films. The *inset* shows the magnified region of (002) peak

Table 1 Structural parameters of undoped and Na doped ZnO thin films

Na (at.%)	2θ (°)	FWHM (°)	D (nm)	c (Å)	σ (GPa)
0	34.543	0.408	20.4	5.1889	0.761
3	34.509	0.386	21.6	5.1939	0.537
6	34.485	0.442	18.8	5.1974	0.358
9	34.468	0.463	18.0	5.1999	0.269

with their *c*-axes perpendicular to the deposition substrate plane. From the XRD spectra, it is evident that there are no extra peaks corresponding to Na metal or sodium oxides, within the apparatus detection limit, indicating that as synthesized samples are single phase and Na$^+$ might substitute Zn^{2+} or incorporate into interstitial sites in the ZnO lattice. In addition, the inset of Fig. 1 shows that as Na content increases from 0 to 9 at.% the (002) peak positions shift toward lower angles as compared to the undoped ZnO. Our results are in agreement with previous works of Wang et al. [23] who reported that with an increase of Na content from 0 to 24 at.%, the (002) peak position of Na doped ZnO thin films shifts to the lower diffraction angle side. Moreover, it is clearly seen that Na doping strongly affects the peak intensity. When the doping concentration is 3 at %, the intensity of (002) peak of the film is the strongest demonstrating its better crystal quality and higher preferential c-axis orientation. With the increase of Na-doping concentration, the (002) peak intensity is significantly reduced. It is evident that 3 at.% Na-doping greatly improved the crystallization quality of the ZnO thin film. In addition, this result suggests that suitable Na doping will be helpful in obtaining a preferable c-axis orientation of the ZnO film.

The lattice constant *c* can be calculated from the XRD data by using the following formula:

$$c = \frac{\lambda}{\sin \theta} \tag{1}$$

where $\lambda = 0.15406$ nm is the *X*-ray wavelength and θ is the Bragg angle of (002) peak. The results are summarized in Table 1; they show that the lattice constants *c* of the Na doped ZnO are larger than those of the undoped one. This result may be attributed to the incorporation of the Na ions into substitutional positions. It is believed that the substitution of smaller Zn^{2+} (0.74 Å) with larger Na$^+$ (1.02 Å)

leads to an increase in the lattice constant. Similar trends have been reported by Wang et al. [23]. It is also possible that interstitial incorporation of Na ions into the lattice parameters contributes to the increasing of the c parameter.

For hexagonal ZnO crystals with wurtzite structure and highly *c*-axis preferred orientation, the in-plane residual stress (σ) of the films can be calculated from a biaxial strain model analysis using the following formula [24]:

$$\sigma = \frac{2C_{13}^2 - C_{33}(C_{11} + C_{12})}{2C_{13}} \times \frac{(c - c_0)}{c_0} \tag{2}$$

where $c_0 = 5.2066$ Å is the unstrained lattice constant of ZnO along the *c*-axis according to the XRD assignment by the American Society for Testing and Materials ASTM: 36-1451, *c* is the lattice parameter of films obtained from XRD result, $C_{13} = 104.2$ GPa, $C_{33} = 213.8$ GPa, $C_{11} = 208.8$ GPa and $C_{12} = 119.7$ GPa are the elastic stiffness constant values of ZnO crystal [25]. The positive value of stress indicates that the films are in a state of tensile stress. As can be seen from Table 1, the biaxial tensile stress in the films is weak and was found to decrease from 0.761 to 0.269 GPa with Na doping indicating that the tensile stress associated with the undoped ZnO film was progressively reduced. This behavior puts into evidence that both undoped and Na doped ZnO films show very good adherence to quartz substrates [26].

Average crystal sizes were estimated from the (002) peak using the well-known Scherer's formula [27]:

$$D = \frac{0.9\lambda}{\beta \cos \theta} \tag{3}$$

where D and β are the average crystallite size and the full width at half maximum (FWHM) of the XRD peak signal with peak position at θ in radian, respectively. The calculated results are listed in Table 1. It can be seen that the average crystal size increases from 20.4 to 21.6 nm as Na doping concentration increases from 0 to 3 at. %, indicating that incorporation of Na significantly enhances the crystalline quality of ZnO thin film. This increase in the crystallite size may be because Na ions can occupy both the lattice and interstitial site, due to the difference of ionic charge and radius between Zn^{2+} ion and Na$^+$ ion, which

probably favors the preferential growth of larger sized crystallites and enhances the crystallinity [28]. However, opposite tendency is observed for higher Na doping levels i.e., the crystallite size is found to decrease with Na concentration from 18.8 nm (6 at.%) to 18.0 nm (9 at.%).This result may be related to the nucleation mechanism of ZnO and/or the segregation of Na atoms at the grain boundaries. As Na concentration increases, the number of nucleations of ZnO enhances leading to a reduction in the crystallite size. Similar trends have been observed in ZnO using Na and other dopants such as K [29, 30]. The increase of Na concentration will enhance the nucleation of the ZnO phase, which leads to a reduction in the crystal grain size.

Raman spectroscopy is also performed to elucidate the structural characteristics of the prepared samples. Figure 2a–d illustrate Raman spectra of the undoped and Na doped ZnO thin films at different concentrations recorded in the range of wavenumbers 200–1000 cm^{-1}. The broad peaks located around 488, 600 and 790 cm^{-1} are present in all spectra of our samples and are optical phonon modes excited from the quartz substrate [31]. As shown in Fig. 2a, the Raman spectra of the undoped ZnO film displays a peak at about 437 cm^{-1} assigned to the high frequency branch of the E_2(high) mode, which is a characteristic peak for the hexagonal phase of ZnO [32]. The asymmetric nature of this peak is also typical of the Raman active mode specially observed in wurtzite structure. This observation is in good agreement with the work of Shinde et al. [33] who recorded a similar peak at ~ 437 cm^{-1} from the Raman spectra of

their ZnO thin films grown by spray pyrolysis technique. All the doped ZnO films reveal similar scattering peaks observed at around 437.7 ~ 439 cm^{-1} assigned to ZnO, indicating that they have identical crystal structures as confirmed by XRD. The absence of the peaks at 410 and 580 cm^{-1} assigned to E_1 (TO) and E_1 (LO) modes [34] in the Raman spectra of undoped and Na doped ZnO films demonstrates, on the one hand, the development of preferred c-axis orientation in these films [28]. On the other hand, it may be used as an indicator for their high crystalline quality since the peak at 580 cm^{-1} is associated with impurities and the formation of crystal defects such as oxygen vacancies and zinc interstitials [35]. From Fig. 2b–d it is evident that the crystallinity of the ZnO film was affected by the Na doping concentration. The peak appearing at 437.7 cm^{-1} in the Raman spectrum of the Na doped ZnO film at 3 at.% concentration exhibits higher intensity with smaller FWHM relative to other samples, which means that its crystal quality is the highest in good agreement with XRD results. In addition, it can be seen that the E_2 (high) peak position of undoped ZnO film shift from 437 to 437.7 cm^{-1}, 438.4 and 439 cm^{-1} for the ZnO films doped at 3, 6 and 9 at.% Na, respectively. This shift in the E_2 (high) Raman peak to longer wavenumber with doping could be explained by the decrease in the stress developed in the ZnO films [36]. This result is consistent with the observed lattice parameters changes and the progressive reduction of residual stress in doped ZnO films with increasing Na concentration determined from XRD data.

Fig. 2 Raman spectra of Na doped ZnO thin films:
a Na = 0 at.%, **b** Na = 3 at.%,
c Na = 6 at.% and
d Na = 9 at.%
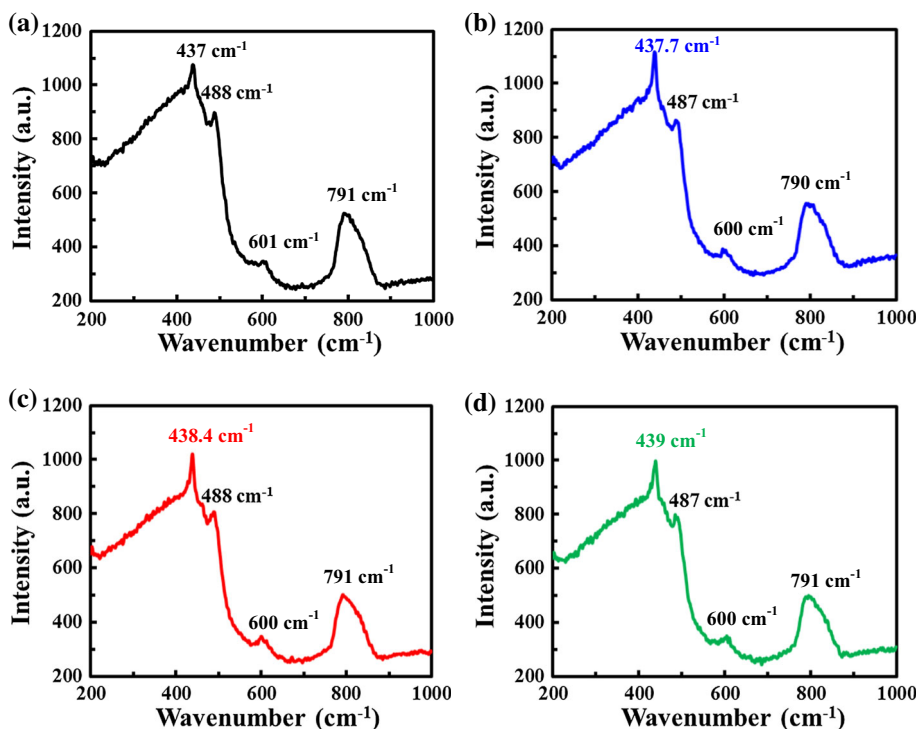
Finally, the Raman spectra of Na doped ZnO thin films do not illustrate additional vibrational mode corresponding to a secondary phase demonstrating that Na atoms are well incorporated into the ZnO lattice [37], consistent with the abovementioned XRD results.

Two-dimensional (2D) AFM images of pure and doped ZnO thin films at different Na concentration are depicted in Fig. 3. It is clearly seen that the undoped ZnO thin film exhibits uniformly distributed like spherical grains of varying sizes. The surface morphology of 3 at.% Na doped ZnO film presents uniform distribution of densely packed well-defined grains with well-defined grain boundaries of more or less uniform size. The AFM images of the ZnO films doped at 6 and 9 at.% Na show uniform dense distribution of smaller grains with some pores on the surface. The root mean square surface roughness (R_{rms}) of the films was determined using the Gwyddion analysis software [38]. Furthermore, the roughness value was obtained averaging the values obtained over three different images. From the data analyses, one can infer R_{rms} values of 3.23, 4.32, 2.81 and 2.49 nm, respectively, corresponding to ZnO thin films grown with 0, 3, 6 and 9 at.% of Na. It can be seen that the film prepared with Na doping

concentration of 3 at.% exhibits the highest roughness value as compared to the other samples. Moreover, average grain size of the thin films increases initially, and then decrease with increasing Na concentration. These observations are in a good agreement with XRD results.

3.2 Electrical and optical properties

In order to investigate the electrical properties of the pure and Na-doped ZnO thin films, Hall-effect measurements were carried out at room temperature using the four-probe Van der Pauw configuration. The measurements were repeated several times for all the samples in order to examine the reliability and repeatability of the conduction of the films. The results are summarized in Table 2. It shows that the electrical properties of ZnO films are dependent on Na doping content. ZnO thin films grown with 0 and 9 at.% of Na exhibit n-type conduction, whereas the ZnO thin film prepared from solution with 3 at.% of Na behaves as a p-type semiconductor. The values for hole concentration, mobility and electrical resistivity are 4.9×10^{16} cm^{-3}, 0.15 cm^2 V^{-1} s^{-1} and 826.47 Ω cm, respectively. In contrast, the sample doped at 6 at.%

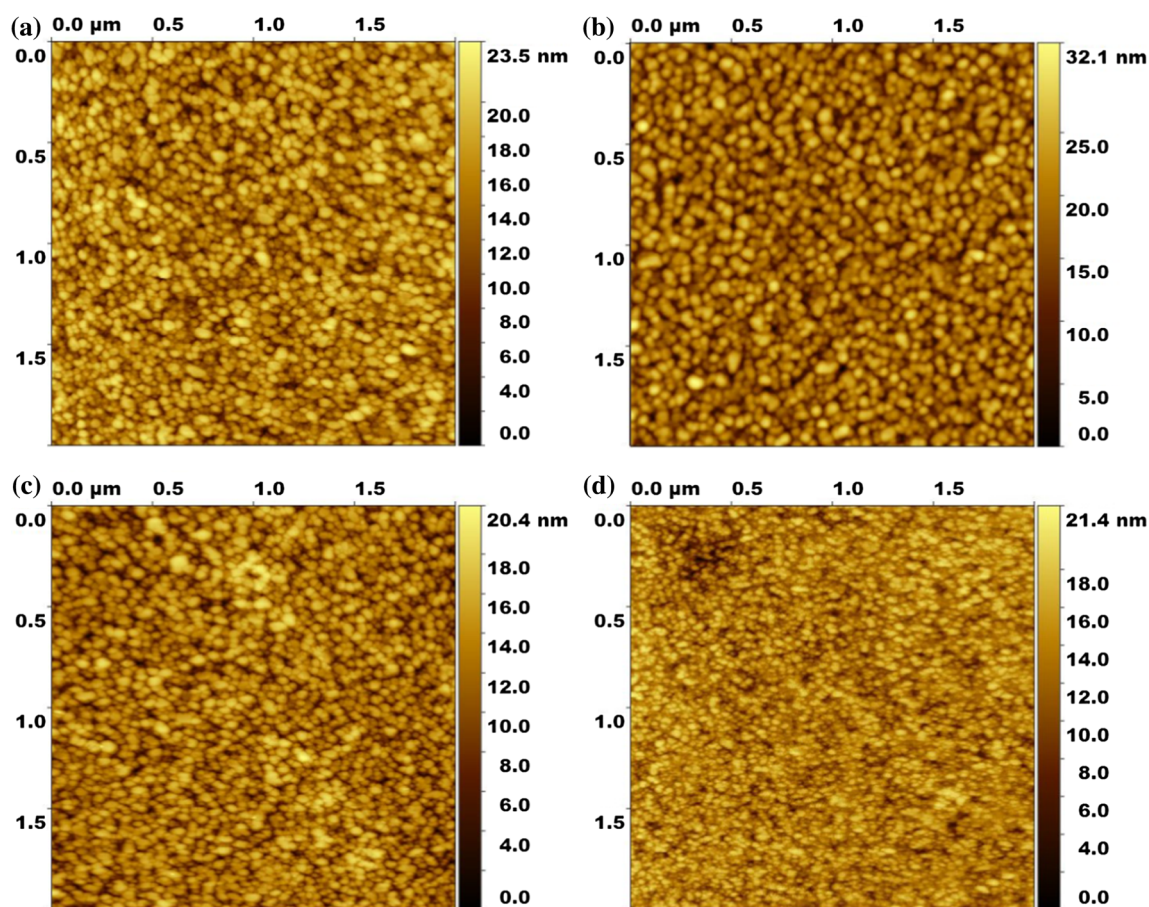**Fig. 3** 2D AFM images of Na doped ZnO thin films: **a** Na = 0 at.%, **b** Na = 3 at.%, **c** Na = 6 at.% and **d** Na = 9 at.%

Table 2 Electrical properties of undoped and Na doped ZnO thin films

Na (at.%)	Carrier concentration ($\times 10^{14}$ cm^{-3})	Mobility (cm^2 V^{-1} s^{-1})	Resistivity (Ω cm)	Conduction type
0	1.61	10.66	3629.06	n
3	486	0.15	826.47	p
6	2.74	1.81	12554.95	p/n
9	0.167	7.25	51419.	n

exhibits unambiguous conduction demonstrating that hole and electron densities are of the same order of magnitude. It is believed that the p-type conductivity of the ZnO doped at 3 at.% is due to the presence of Na$_{Zn}$ acceptors defects as reported by Lin et al. [12]. In our case and taking into consideration the fact that the growth environment controls the concentration of native defects in ZnO and since the sol used for ZnO deposition was rich on oxygen; one may anticipate a relatively high V$_{Zn}$ density in the samples. Hence, for relatively moderate Na doping (3 at.%), the Na atoms substitute to V$_{Zn}$ and consequently Na$_{Zn}$ acceptors form in this sample. This result is in good agreement with literature [18]. The substitution of the Na in the zinc sites is also evident from XRD results. The increase of Na doping concentration, leads to the formation of some compensating Na$_i$ defects (existence of Na$_{Zn}$–Na$_i$ complexes) causing unambiguous conduction type [17]. Wan et al. [39] have theoretically predicted that Na$_{Zn}$ acceptors and Na$_i$ donors can easy form in the Na-doped ZnO. As a result, in Na-doped ZnO, Na$_i$ is in the material to compensate the Na$_{Zn}$ defect which always behaves as acceptor. Further increase in Na doping up to 9 at.% enhances Na$_i$ donors defects leading to n-type conduction. It is noticeable that the resistivity decreases with increasing Na content up to 3 at.% and the excessive Na doping will lead to higher resistivity. Carrier concentration has the inverse behavior. The decrease in the resistivity and the increase of the hole concentration can be explained by the improvement of crystal quality. As the Na content further increases, the crystal quality is degraded resulting in an increase of the resistivity and a decrease in carrier concentration [11].

Figure 4a depicts the optical transmission spectra of the undoped and Na doped ZnO films deposited on quartz substrates. As can be seen, all the samples are highly transparent in the visible and near-infrared regions. Undoped ZnO film exhibits an average optical transmittance exceeding 81 % in the visible region; whereas doped samples have an average transmittance of about 78, 79 and 77 % for Na doping concentration of 3, 6 and 9 at.%, respectively. These results suggest that Na doping has no significant effect on the transparency of the ZnO thin films. However, as can be seen in the inset of Fig. 4a, the UV absorption edge of Na doped film at 3 at.% shows a clearly red-shift compared to the pure ZnO film. Moreover, as Na

doping content increases to 9 at.%, a blue shift of the absorption edge is observed demonstrating that the optical band gap E$_g$ of the ZnO film would be affected by the Na doping as will be discussed below.

The band gap energies (E$_g$) of all samples were determined by using the method based on the derivative of the transmittance (T) with respect to energy (E), dT/dE, taking into account that ZnO is a direct band gap semiconductor as described in our previous works [40, 41]. This accurate technique has been also used by Wang et al. [42]. According to the measured transmission spectra, the dT/dE curves of undoped and Na-doped ZnO thin films at different concentrations are illustrated in Fig. 4b. Our analysis indicates that the E$_g$ of undoped ZnO film was found to be 3.267 eV. In comparison, the band gap energies of the films doped at 3, 6 and 9 at.% Na are 3.250, 3.280 and 3.289 eV, respectively. These values are very close to the ZnO band gap value reported by Jun et al. [43]. It can be noted that the band gap energy value decreased for the sample with a 3 at.% Na doping concentration. This behavior may be ascribed to the increase in the crystallite size and/or demonstrated the p-type conductivity of the film. When Na concentration increases from 0 to 3 at.%, the native donor defects in the undoped film are compensated by Na$_{Zn}$ defects inside the band gap. These defects form shallow acceptor levels above the valence band maximum (VBM) leading to p-type conduction. Therefore, larger hole concentration results in the reduction of E$_g$ in the sample doped at 3 at.%. Kumar et al. [28] have also reported that band gap reduction in their Na-doped ZnO nanocrystalline thin films synthesized using sol–gel spin coating technique confirms the p-type conduction. While, the band gap widening of Na-doped ZnO films at 6 and 9 at.% could be attributed to the decrease in crystallite size and/or n-type carrier concentration as has been reported by Wang et al. [23] and Lai et al. [20]. In the one hand the reduction of crystallite size with the increase of the Na level from 6 to 9 at.% leads to the increase of E$_g$ due to quantum size effect. In the other hand, the increase in Na doping up to 9 at.% enhances Na$_i$ donors defects which may induce impurity levels near the conduction band minimum (CBM). These Na$_i$ defects compensate Na$_{Zn}$ acceptors leading to the increase in electron concentration. Therefore, the conductivity is changed to be n-type and the band gap increases.
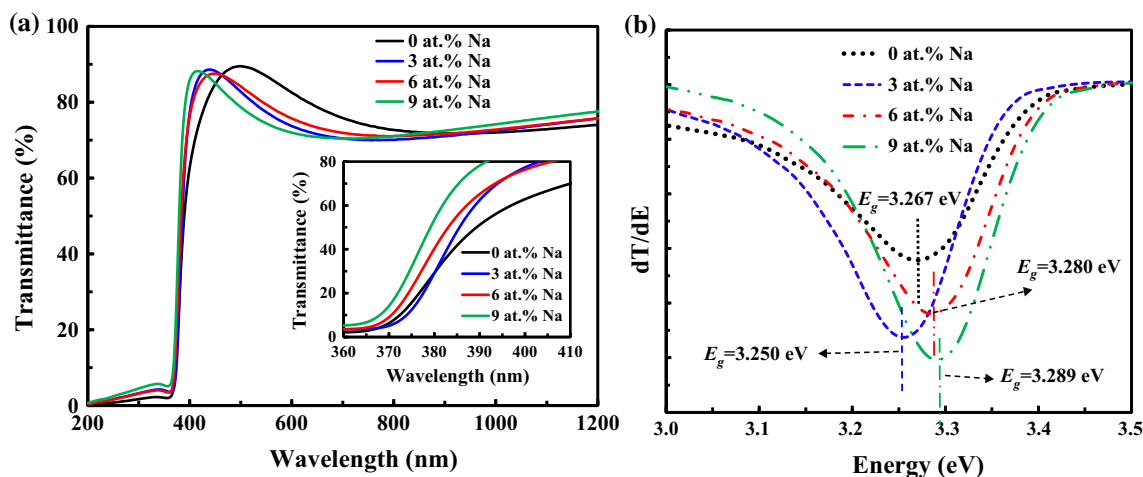
Fig. 4 **a** UV–Vis–NIR transmittance spectra of undoped and Na-doped ZnO thin films, **b** Plots of the derivative of the transmittance with respect to energy of undoped and Na-doped ZnO thin films. The *inset* shows the magnification of absorption edge region

Figure 5 displays photoluminescence spectra recorded at room temperature on undoped and Na doped ZnO thin films; the inset depicts the UV emission region. All the films present only a near-band-edge (NBE) emission. It is observable that this emission depends on the Na content. In particular, the Na doping affects the intensity and the position of this UV emission. The emission of the sample doped at 3 at.% centered at 382 nm (3.24 eV) is broad and red shifted indicating a decrease in band gap. The reduction of the band gap may be due to the p-type conduction [44]. PL results of p-type Na-doped ZnO have also been reported by Ghosh et al. [45]. They found that the UV emission becomes broad and red shifted due to the convergence of the electronic transitions from the conduction band minimum to both shallow Na_{Zn} acceptor states and to the valence ban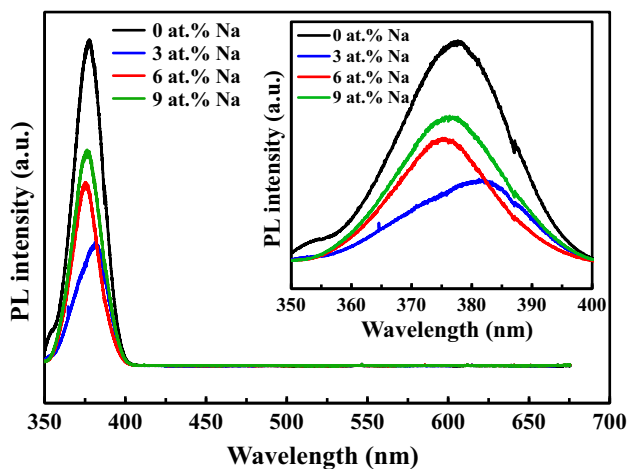d (band to band transition). It is largely accepted that the Na_{Zn} defect creates shallow acceptor states above the VBM [45]. Hence, the broad UV emission observed in the 3 at.% Na is the result of the superposition of the radiative electronic transition from the CBM to Na_{Zn} acceptors and the transition from CBM band to VBM. Based on this reported work, the broadening of the UV emission of the sample doped at 3 at.% Na is probably due to the existence of Na_{Zn} acceptor defect responsible of the p-type conduction. Moreover, it can clearly be seen that the highest intensity of the UV emission is recorded from the undoped sample while the lowest one is obtained from the film doped at 3 at.%. In particular, the UV emission intensity of undoped and the Na doped at 9 at.% is higher than those of the samples doped at 3 and 6 at.%. Lopatiuk-Tirpak et al. [46] have reported that the NBE emission in Sb-doped p-type ZnO decrease with increasing hole concentration due to the reduction in radiative recombination rates as more disorder is introduced into the ZnO lattice by large-radius Sb atoms. In addition, Vanheusden et al. [47] have explained the decrease in PL intensity in Pb-doped n-type ZnO by the decrease in electron concentration. Therefore, in our case the behavior of UV emission may be associated to carrier type and carrier concentration. Therefore, since the undoped and the Na-doped ZnO at 9 at.% are n-type, the decrease of the UV emission of the latter sample is due to the reduction of the electron concentration as shown in Table 2. However, the transformation of conductivity from n-type to p-type in the sample doped at 3 at.% leads to the more decrease in electron density and the hole concentration becomes larger than that of electrons leading to the further decrease in the UV emission of this film.

In order to confirm the existence of Na acceptors responsible of p-type conduction of the 3 at.% Na doped ZnO thin film sample, PL measurements were also carried
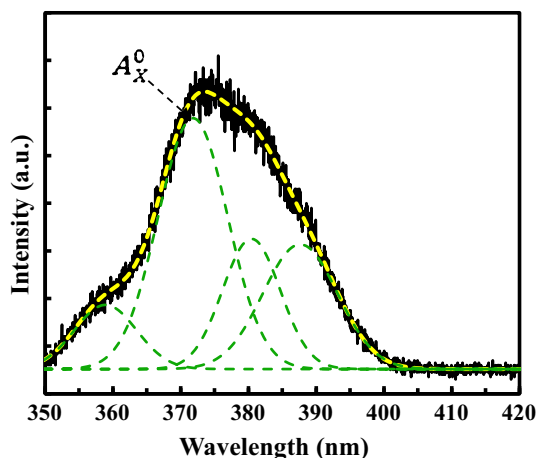

Fig. 5 Room temperature PL spectra of undoped and Na-doped ZnO thin films. The *inset* shows the magnification of the UV emission region

Fig. 6 PL spectrum of 3 at.% Na-doped ZnO thin film at 77 K

out at 77 K and the result is depicted in Fig. 6. As can be seen from this figure, the Guassian deconvolution of the PL spectrum puts into evidence an intense emission at 3.35 eV. Liu et al. [13] have also observed an Na-related peak at 3.35 eV in Na doped ZnO microwires, which they ascribed to A_X^0 acceptor-bound excitons. Therefore, in our case the p-type behavior of the Na-doped ZnO at 3 at.% may be attributed to the formation of Na_{Zn} defects. These results are in agreement with Hall-effect measurements. The absence of the visible emission indicates a high quality of the sample and hence the small defects densities of some native defects such as oxygen vacancy and zinc interstitials [48], which agrees very well with the results obtained from Raman analysis.

4 Conclusion

Undoped and Na-doped ZnO thin films were deposited on quartz substrates by the sol–gel dip-coating process. Microstructure, surface topography, electrical and optical properties of the thin films have been investigated. XRD analysis revealed that all the thin films possess a hexagonal wurtzite structure. The 3 at.% Na-doped ZnO thin film exhibited better crystallinity and high c-axis preferred orientation. From Raman Spectroscopy all the peaks observed in undoped and Na-doped samples matched with the Raman active modes assigned to the hexagonal phase of ZnO. According to AFM images, the samples display a homogeneous distribution of particles over the surface. The average grain size and surface roughness were found to increase initially and then decrease with increasing Na concentration, which is consistent with the XRD result. Hall-effect measurements revealed that p-type conductivity was observed only on the 3 at.% Na-doped sample with a hole concentration, Hall mobility and electrical resistivity of about

$4.9 10^{16}$ cm^{-3}, 0.15 cm^2 V^{-1} s^{-1} and 826.47 Ω cm, respectively. UV–Vis–NIR transmittance spectra indicated that all the ZnO films were highly transparent with average visible transmission values ranging from 77 to 81 %. Moreover, with the increase of doping concentration, a change of the optical absorption edge from red shift to blue shift is observed. Room temperature PL results put into evidence that the undoped sample exhibit the highest UV emission intensity whereas the p-type Na doped ZnO film at 3 at.% emits the lowest one. Furthermore, the p-type conductivity of the 3 at.% Na-doped ZnO film was also confirmed by the PL measurement at 77 K.

References

1. Z. Zang, A. Nakamura, J. Temmyo, Opt. Express **21**(9), 11448 (2013)
2. Z. Zang, X. Zeng, J. Du, M. Wang, X. Tang, Opt. Lett. **41**, 3463 (2016)
3. M.M. Momeni, Indian J. Chem. Sect. A **55**, 686 (2016)
4. J.C. Fan, K.M. Sreekanth, Z. Xie, S.L. Chang, K.V. Rao, Prog. Mater. Sci. **58**, 874 (2013)
5. E.C. Lee, K.J. Chang, Phys. Rev. B **70**, 115210 (2004)
6. C.H. Park, S.B. Zhang, S.H. Wei, Phys. Rev. B **66**, 073202 (2002)
7. Z.C. Feng, *Handbook of Zinc Oxide and Related Materials: Materials*, vol. 1 (CRC press Taylor and Francis, New York, 2013), p. 93
8. J. Huang, J. Qi, Z. Li, J. Liu, Nanotechnology **24**, 395203 (2013)
9. S.S. Lin, H.P. He, Y.F. Lu, Z.Z. Ye, J. Appl. Phys. **106**, 093508 (2009)
10. H. He, S. Lin, G. Yuan, L. Zhang, W. Zhang, L. Luo, Y. Cao, Z. Ye, S.T. Lee, J. Phys. Chem. C **115**, 19018 (2011)
11. Z. Zheng, Y.F. Lu, Z.Z. Ye, H.P. He, B.H. Zhao, Mater. Sci. Semicond. Proc. **16**, 647 (2013)
12. S.S. Lin, Z.Z. Ye, J.G. Lu, H.P. He, L.X. Chen, X.Q. Gu, J.Y. Huang, L.P. Zhu, B.H. Zhao, J. Phys. D Appl. Phys. **41**, 155114 (2008)
13. W. Liu, F. Xiu, K. Sun, Y.H. Xie, K.L. Wang, Y. Wang, J. Zou, Z. Yang, J. Liu, J. Am. Chem. Soc. **132**, 2498 (2010)
14. Y. Li, Y. Zhang, H. He, Z. Ye, J. Jiang, L. Cao, Mater. Lett. **76**, 81 (2012)
15. L.L. Yang, Z.Z. Ye, L.P. Zhu, Y.J. Zeng, Y.F. Lu, B.H. Zhao, Electron. Mater. **36**, 498 (2007)
16. W. Ko, S. Lee, G. Baek, J.P. Hong, Curr. Appl. Phys. **14**, S103 (2014)
17. X.H. Pan, Y.S. Zhou, S.S. Chen, P. Ding, B. Lu, J.Y. Huang, Z.Z. Ye, J. Cryst. Growth **404**, 54 (2014)
18. Y.F. Lu, K.W. Wu, Y.J. Zeng, Z.Z. Ye, J.Y. Huang, L.P. Zhu, B.H. Zhao, Chem. Phys. Lett. **582**, 82 (2013)
19. K.J. Kim, P.B. Kreider, C. Choi, C.H. Chang, H.G. Ahn, RSC Adv. **3**, 12702 (2013)
20. J.J. Lai, Y.J. Lin, Y.H. Chen, H.C. Chang, C.J. Liu, Y.Y. Zou, Y.T. Shih, M.C. Wang, J. Appl. Phys. **110**, 013704 (2011)
21. F. Boudjouan, A. Chelouche, T. Touam, D. Djouadi, S. Khodja, M. Tazerout, Y. Ouerdane, Z. Hadjoub, J. Lumin. **158**, 32 (2015)
22. F. Boudjouan, A. Chelouche, T. Touam, D. Djouadi, Y. Ouerdane, Mater. Sci. Semicond. Proc. **41**, 382 (2016)

23. L.W. Wang, F. Wu, D.X. Tian, W.J. Li, L. Fang, C.Y. Kong, M. Zhou, J. Alloys. Compd. **623**, 367 (2015)
24. M.K. Puchert, P.Y. Timbrell, R.N. Lamb, J. Vac. Sci. Technol. **14**, 2220 (1996)
25. M. Chen, Z.L. Pei, C. Sun, L.S. Wen, X. Wang, J. Cryst. Growth **220**, 254 (2000)
26. S.B. Yahia, L. Znaidi, A. Kanaev, J.P. Petitet, Spectrochim. Acta A **71**, 1234 (2008)
27. J.I. Langford, A.J.C. Wilson, J. Appl. Crystallogr. **11**, 102 (1978)
28. S. Kumar, R. Thangavel, J. Sol–Gel Sci. Technol. **67**, 50 (2013)
29. J. Lü, K. Huang, J. Zhu, X. Chen, X. Song, Z. Sun, Phys. B **405**, 3167 (2010)
30. L. Xu, X. Li, J. Yuan, Superlattice Microstruct. **44**, 276 (2008)
31. R.S. Sreedharan, V. Ganesan, C.P. Sudarsanakumar, K. Bhavsar, R. Prabhu, V.P.P.M. Pillai, Nano Rev **6**, 26759 (2015)
32. M. Koyano, P. Quocbao, L.T. Thanbbinh, L. Hongha, N. Ngoclong, S. Katayama, Phys. Stat. Sol. A **193**, 125 (2002)
33. S.S. Shinde, P.S. Shinde, V.G. Sathe, S.R. Barman, C.H. Bhosale, K.Y. Rajpure, J. Mol. Struct. **984**, 186 (2010)
34. K.A. Alim, V.A. Fonoberov, M. Shamsa, A.A. Balandin, J. Appl. Phys. **97**, 124313 (2005)
35. S.J. Chen, Y.C. Liu, Y.M. Lua, J.Y. Zhang, D.Z. Shen, X.W. Fan, J. Cryst. Growth **289**, 55 (2006)
36. O. Lupan, T. Pauporté, L. Chow, B. Viana, F. Pellé, L.K. Ono, B.R. Cuenya, H. Heinrich, Appl. Surf. Sci. **256**, 1895 (2010)
37. H.Q. Ni, Y.F. Lu, Z.Y. Liu, H. Qiu, W.J. Wang, Z.M. Ren, S.K. Chow, Y.X. Jie, Appl. Phys. Lett. **79**, 812 (2001)
38. D. Nečas, P. Klapetek, Cent. Eur. J. Phys. **10**, 181 (2012)
39. Q. Wan, B. Shao, Z. Xiong, D. Li, G. Liu, Appl. Mech. Mater. **665**, 124 (2014)
40. M. Dehimi, T. Touam, A. Chelouche, F. Boudjouan, D. Djouadi, J. Solard, A. Fischer, A. Boudrioua, A. Doghmane, Adv. Condens. Matter Phys. **2015**, 740208 (2015)
41. T. Touam, M. Atoui, I. Hadjoub, A. Chelouche, B. Boudine, A. Fischer, A. Boudrioua, A. Doghmane, Eur. Phys. J. Appl. Phys. **67**, 30302 (2014)
42. M. Wang, E.J. Kim, S. Kim, J.S. Chung, I. Yoo, E.W. Hahn, S.H. Shin, C. Park, Thin Solid Films **516**, 1124 (2008)
43. M.C. Jun, J.H. Koh, Nanoscale Res. Lett. **7**, 294 (2012)
44. M. Futsuhara, K. Yoshioka, O. Takai, Thin Solid Films **317**, 322 (1998)
45. S. Ghosh, G.G. Khan, S. Varma, K. Mandal, Appl. Mater. Interface **5**, 2455 (2013)
46. O. Lopatiuk-Tirpak, W.V. Schoenfeld, L. Chernyak, F.X. Xiu, J.L. Liu, A. Osinsky, P. Chow, Appl. Phys. Lett. **88**, 202110 (2006)
47. K. Vanheusden, W.L. Warren, J.A. Voigt, C.H. Seager, D.R. Tallant, Appl. Phys. Lett. **67**, 1280 (1995)
48. A.B. Djurisic, Y.H. Leung, Small **2**(8–9), 944 (2006)